Title: Biomolecular condensates form through the thermodynamics of rapid binding interactions

Authors: J. Matthew Dubach

Affiliations:
Institute for Innovation in Imaging, Department of Radiology, Massachusetts General Hospital, Harvard Medical School, Boston, MA

Abstract: Biomolecular condensates are intracellular membrane-less accumulations of proteins and other molecules at a higher concentration than the rest of the cell. The recent characterization of condensates as liquid-like assemblies has stimulated profound interest in how physical properties of condensates impact molecular biology. Intriguingly, condensates have been shown to be essential to multiple different cellular processes and underlying aspects of various diseases. Yet, the physics of condensate formation remains unsolved. Here, the binding model solves condensate formation thermodynamics demonstrating that binding interactions under certain conditions induce spontaneous condensate formation. Condensate reentrance, the energy of condensate formation and the binding affinity and binding dynamic limits of condensate molecules are all captured in the binding model. Overall, the binding model, while certainly incomplete, describes the energetic properties of complex coacervation, biomolecular condensates and aggregate formation.

One Sentence Summary: Intrinsically disordered protein binding governs biomolecular condensate formation.

Main Text:
Biomolecular condensates are characterized by: their ability to rapidly exchange most components with the surrounding environment (*1*); their liquid-like properties that allow them to flow, move and merge (*2*); their dependency on environmental conditions (*3*); the presence of oligonucleotides (*4*); the abundance of fully intrinsically disordered proteins or proteins that contain intrinsically disordered regions (IDR) (*5*); their ability to rapidly form or dissolve (*2*); and, in cells, inclusion of multiple proteins (*6*). Condensates are thought to be essential to cellular biology and critical in myriad human disease (*7*). However, the physical properties that produce condensate formation remains unclear.

Fundamentally, biomolecular condensates must generate an overall system free energy that is lower than dilute distribution of components. Thermodynamically, condensates produce a lower entropy of mixing, therefore, since condensates form spontaneously, energetic advantages that overcome this entropic cost are required. Initial considerations of biomolecular condensates modeled their formation as liquid-liquid phase separation (LLPS) (*2*). LLPS occurs when the entropic cost of condensation is less than the entropic loss due to restricted molecular orientations of the abundant liquid surrounding each of the less-abundant molecules. But aspects of condensates do not fit canonical LLPS models (*8, 9*), therefore properties of polymer physics, such as Flory-Huggins interaction energies (*10, 11*), have been used to describe the energetic landscape of condensates. Discovery that the abundance of polar amino acids found in IDRs are drivers of condensate formation (*12, 13*) suggested that Flory-Huggins was a good model for condensation. Yet, observations that altered order of amino acids (*14*) and replacement of charged amino acids (*15*) prevents condensate formation led to the "stickers and spacers" model.

The sticker and spacer model relies on multivalent interactions of molecules that form condensates (*16*). Gelation (or percolation) (*12, 17*) of these interactions along with phase separation (*9*) is proposed to induce condensation. Stickers can be single amino acids but have also been demonstrated with diverse molecules such as polymeric SUMO (*18*). Observations of the sequence dependency on dense phase

concentration and material properties of condensates (*19, 20*) and loss of just a single sticker impacting the condensate saturation concentration (*21*) suggest that these binding interactions are essential. However, in the sticker and spacer model, how condensates spontaneously form, the impact of the complex biological environment (*9*) and why single amino acid mutations (*15*) disrupt condensate formation remain unanswered. Here, the energetic impact of binding in the absence of a multivalency requirement is considered as a driver of condensate formation (the binding model). Complementary to Flory-Huggins and sticker and spacer, this model considers condensation driven by a single, integrated binding affinity.

INCREASED BINDING IN CONDENSATES OVERCOMES THE ENTROPIC COST

Recent results show that IDR proteins can bind with rapid dynamics (*22-24*). Spontaneous binding arises through a reduction in free energy with affinities that are defined by a steady state dissociation constant (**Fig. 1A**), shown here for simplicity is homotypic binding. The steady state fraction bound of interacting molecules is defined by the total concentration and dissociation constant (*25*) and can be generalized to any system through dividing the concentration by the affinity (here protein is used to give $[\text{protein}]_{total}/K_d$) (**Fig. 1B**). At higher $[\text{protein}]_{total}/K_d$ ratios a larger fraction will be bound. Condensation in a system generates both dilute and concentrated regions where, driven by $[\text{protein}]_{total}/K_d$, binding is higher in condensates but lower in dilute regions (**Fig. 1C**). Summing the volume-weighted, K_d-governed binding in both regions produces the total fraction bound in the system. Since protein in a diffuse state is largely unbound at low $[\text{protein}]_{total}/K_d$, transition into condensates generates a higher fraction of bound molecules (**Fig. 1D**). The total fraction of bound protein in the system is therefore a function of the condensate partition function and the $[\text{protein}]_{total}/K_d$ ratio (fig. S1A). An effective K_d can be calculated from the total fraction bound in the presence of condensates (fig. S1B) to determine the change in free energy from increased binding as a function of $[\text{protein}]_{total}/K_d$ (**Fig. 1E** and eq. 1). However, the entropic cost of de-mixing that arises when condensates are present also increases with partition coefficient (**Fig. 1F** and eq. 2). Therefore, integrating the decrease in free energy through increased binding and the entropic cost of de-mixing generates the total energetic impact of condensation as a function of the partition coefficient and $[\text{protein}]_{total}/K_d$ (**Fig. 1G** and fig. S1C). The energy minimum for each $[\text{protein}]_{total}/K_d$, which has a dependency on condensate volume fraction (fig. S1D), predicts the $[\text{protein}]_{total}/K_d$ ratios that will generate spontaneous, thermodynamically favorable condensates (**Fig. 1I**).

The binding model of condensation predicts that condensates are not formed at $[\text{protein}]_{total}/K_d$ ratios above 10^{-1}. Therefore, increasing the protein concentration or decreasing the K_d in a system with stable condensates at $[\text{protein}]_{total}/K_d < 10^{-1}$ can induce condensate reentrance (loss of condensates). This reentrance phenomenon is not predicted by existing condensate thermodynamic models (*9*) and represents a simple test of the binding model. Thus, condensates were formed with K_{20} and E_{20} peptides at a 1:1 molar ratio, maintaining charge neutrality, similar to previous results (*26*). These condensates exhibited both merging and spontaneous disappearance (fig. S2A). At 350 mM NaCl in 10 mM Tris buffer, pH 8.0, condensation demonstrated a concentration saturation (c_{sat}, the concentration above which condensates form) at 1 mM, but also reentrance at 15 mM (**Fig. 2A**).

High salt concentrations can induce condensate reentrance (*27*), suggesting that the abundance of ions impacts the free energy of condensate formation. Intriguingly, binding of two oppositely charged polyions primarily arises from the gain in entropy of counterion release and binding can be disrupted by high counterion concentrations that lower this entropic advantage (*28*). Therefore, if binding is the driver of condensate formation, the presence of counterions will disrupt the energetic advantage of condensation. And, the salt concentration at reentrance will correlate to the total energetic advantage of

binding driven condensation. To test if counterion concentration impacts condensate formation, 1:1 molar mixtures of K_{20} and E_{20} peptides at various peptide and salt concentrations were created and the presence of condensation was determined through DIC imaging. At low concentrations an automated image analysis algorithm quantifying the non-background pixels was used to determine the presence of condensates (fig. S2B). A plot of condensation as a function of salt and peptide concentration demonstrates that condensates reenter solution with a similar energy pattern to the molar free energy calculated from the binding model (**Fig. 2B and C**). At higher concentrations condensates formed upon vigorous mixing but lost homogenous condensation within 10 minutes (fig. S3) suggesting that, at these concentrations, condensation is not energetically favorable, but induced by the added energy of mixing. Based on the predicted condensate reentrance at 10^{-1} $[\text{protein}]_{total}/K_d$ these results suggest that K_{20} and E_{20} bind with a dissociation constant around 100 mM. The formation of condensates as a function of salt and concentration was also determined for K_{30} and E_{30} at 1:1 molar ratios. The 30mer reentrance boundary curve (**Fig. 2D**) displayed a shift toward lower peptide concentrations and higher salt concentrations compared to the 20mer demonstrating higher affinity and predicting that these peptides bind with a K_d around 50 mM. Similar results were found with binding between 1:1 mixtures of K_{10} and D_{10}, where binding is much weaker. However, for the 10mer peptides, a sharp decrease in the reentrance boundary curve at high concentrations could not be established due to limiting counterion concentrations. But, based on c_{sat} for the other peptide condensates, the K_d of K_{10}-D_{10} can be extrapolated to a value around 500 mM (**Fig. 2D**). No condensation was observed with K_4 and E_4, suggesting that the binding affinity is too low to form condensates at the tested concentrations (fig. S2C).

The mechanism of binding-induced counterion release driving condensate formation was further confirmed in unequal molar ratios of E_{30} and K_{30} (fig. S4). At unequal ratios, counterions from the stock solution are unbalanced and condensates are not formed. However, added counterions, which provide ions for release, enabled condensate formation at these unbalanced ratios. The binding model also predicts that the presence of one condensate component above the reentrance $[\text{protein}]_{total}/K_d$ ratio will prevent condensate formation (fig. S5A). This was confirmed experimentally with K_{20} and E_{20} where E_{20} was held above the reentrance concentration and lower concentrations of K_{20} were unable to generate condensates (fig. S5B). However, when both E_{20} and K_{20} were at concentrations below the reentrance concentration, the imbalanced charge ratio from lowering the concentration of just K_{20} did not prevent condensate formation (fig. S5B).

DYNAMIC BINDING IS ESSENTIAL FOR CONDENSATES

K_{50} and E_{50} at a 1:1 molar ratio did not form condensates but rather aggregates (**Fig. 3A**), similar to previous results (*26*). Decreasing the peptide concentration reduced the size of the aggregates but did not generate condensates (fig. S6A). Similarly, increasing the salt concentration also reduced the size of the aggregates, suggesting that aggregates form through polyion binding, but did not generate any condensates (fig. S6B). At 2 mM peptide concentration loss of aggregates occurred at 850 mM NaCl, which was higher than the salt concentration (500 mM) that induced condensate reentrance of E_{30}-K_{30} mixtures at 2 mM, indicating higher affinity binding between the 50mer peptides. Yet, mixtures of 1:1 charge ratios of 2 mM K_{50} and polyE peptides formed condensates with E_{30} and E_{20} but not E_4 (**Fig. 3A**). And, a mixture of 1:1:1 molar ratio of K_{50}-E_{20}-E_{30} also formed condensates at 2 mM (**Fig. 3A**). Reversing the polyions, condensate formation between E_{50} and smaller polyK peptides at neutral total charge was also observed, however, here peptide wetted the glass and condensates rapidly hardened (fig. S7). This hardening occurred for all sizes of polyK, yet condensates were stable when formed with E_{30} and equal charge ratios of K_{20} and K_{10} (fig. S7), demonstrating that interactions with the coverslip impact condensate properties.

Condensate formation with K_{50} at charge neutral ratios only with the smaller polyE peptides suggests that lower affinity binding interactions generate condensates where higher affinity (50mer) do not. This phenomenon cannot be explained by the existing theory that multivalent interactions drive condensation. The lack of condensate formation with K_{50} and E_{50} at multiple concentrations also seemingly refutes the binding model presented here. However, in the binding model the kinetics of binding interactions are essential. Proteins readily exchange between the condensate and dilute region (*29-35*), yet condensation is stable in steady state. In the binding model, condensates consist of both bound and unbound protein. Unbound protein is subject to the entropic force to leave but balanced by the energetic advantage of existing at a high condensate concentration to increase the likelihood of binding (**Fig. 3B**). However, bound protein does not have any energetic advantage to remain within the condensate and is only subject to the gain in entropy upon diffusing into the dilute region. Since flux between the two phases is diffusion driven and the rates of diffusion for bound and unbound will be similar, this imbalanced force will prevent condensation.

Yet, diffusion out of condensates is a dynamic process, and, over time, a bound protein both diffuses and dissociates (**Fig. 3C**). Recent results demonstrate that IDR protein binding and exchange of binding partners in a condensate occurs through extremely fast dynamics, with k_{off} rates greater than 10^6 s^{-1} (*36*). Measured diffusivity rates inside condensates have been reported between 10^{-3} to 10^{-1} $\mu m^2/s$ (*29-34*). Therefore, it is expected that molecules within condensates can exist with dynamics where bound protein dissociates before significant diffusion relative to the size of the typical condensate is achieved (**Fig. 3D**). This phenomenon suggests that the dissociation rate of K_{50}-E_{50} is too slow to form condensates.

THE BINDING MODEL IN PROTEIN-OLIGONUCLEOTIDE CONDENSATES

Condensates can also be generated from mixtures of proteins and oligonucleotides (*37, 38*). Mixtures of K_{20} and a 20mer single stranded DNA (DNA_{20}) produced condensates (**Fig. 4A**). The solubility limitations of DNA prevent 1:1 charge ratio at higher concentrations, thus in this range determination of concentration induced reentrance was performed at uneven molar mixtures. Reentrance was not observed at lower concentrations with the same charge ratio (**Fig. 4B**), confirming that reentrance is driven by concentration and not charge ratio. Both the observed C_{sat} and reentrance concentration where higher for K_{20}-DNA_{20} than K_{20}-E_{20}, suggesting that K_{20} binds DNA_{20} with a larger K_d than E_{20}. Mixtures of K_{20} and a 20mer RNA (RNA_{20}), however, were unable to generate condensates, instead producing aggregates (**Fig. 4C**). Absence of condensates was also found for 1:1 charge ratios of RNA_{20} with K_{50}, K_{30}, K_{10} and K_4 (**Fig. 4C**), with all except K_4 producing aggregates. The absence of condensates remained at lower concentrations as well (fig. S8A). These results suggest that polyK binding to RNA has a much higher affinity than binding to DNA or polyE.

Condensates were formed, however, between polyK and poly(A) RNA (**Fig. 4D**), demonstrating that polyK can form condensates with RNA. As a large polymer, a single molecule of Poly(A) is able to bind multiple molecules of polyK. The binding model predicts that for binding interactions with one molecule having multiple binding sites the reentrance $[protein]_{total}/K_d$ ratio is orders of magnitude higher than for one-to-one binding (fig. S9A), further supporting polyK binding to RNA with high affinity. Condensates for all polyK peptides showed reentrance at both high and low poly(A) ratios (fig. S9B). Existing models of condensate formation between oppositely charged multivalent molecules have predicted that charge imbalance is the driver on reentrance (*39-43*). However, here the span of charge ratios where condensates are stable was dependent on the length of the polyK peptide (**Fig. 4E**),

demonstrating that reentrance with multimeric interactions is likely due to binding energy thresholds and not a charge imbalance.

SUMMARY

Binding interactions between highly flexible molecules are essential to condensate formation (*44*). Experimentally, condensation has been shown to be dependent on properties such as system temperature (*45*), IDR phosphorylation (*46*), and buffering of electrostatic interactions (*5, 27, 47*), all of which alter the energy of binding. The binding model presented here, while quite simple, describes how binding interactions induce spontaneous condensate formation. The binding model is congruent with the majority of experimental results on condensates. The model accurately predicts previously unexpected behavior, such as the intracellular observation that the dilute region concentration and partition coefficient are dependent on the total protein concentration (*48*) (fig. S10). The binding model accurately captures salt induced reentrance (*27*) and indicates that binding energy limitations at imbalanced molar ratios, and not charge imbalance (*40*), induces reentrance, a finding that may clarify transcriptional condensate function (*49*). The model explains complex coacervation (*50*) and the energetic forces governing condensation between oppositely charged molecules (*39*). The binding model also provides insight into disordered protein interactions. As an example, condensate saturation concentrations for FUS family proteins were shown to vary between single micromolar to hundreds of micromolar (*15*), which in the binding model translates to homotypic binding K_d values of single mM to hundreds of mM.

The binding model suggests that rather than physical crosslinks among multivalent proteins being the cause of condensate formation (*51*), any binding interactions provide enough thermodynamic stability to enable condensates. However, the binding model does not exclude the presence of multivalent interactions within a condensate. Rather the model demonstrates that the increased probability of binding (to one or multiple different molecules) within a condensate provides an energetic advantage to overcome the entropic cost of condensation under the right system conditions. The binding model also does not require that the entire length of an IDR be bound. Subsections of a protein may possess the proper binding affinity and dynamics to enable condensation, however unlike the sticker and spacer model, the binding model demonstrates that multiple sticker regions are not required. Therefore, sequence mutations in disordered proteins that prevent condensate formation (*15*) do not remove stickers, but rather alter the binding affinity.

Viewing biological condensate phenomena through the lens of the binding model will have tremendous impact on our understanding of intrinsically disordered proteins. The model suggests that protein sequence (*52*) and post translational modifications (*46, 53*) impact condensates through altered binding affinities. Observations here that K_{50}-E_{50} formed aggregates but K_{50}-E_{20}-E_{30} formed condensates indicates a transition from condensates to aggregates is also governed by binding affinity. This finding suggests that post translational modification induced protein aggregation in neurodegenerative disease (*54, 55*) occurs through increased binding affinity. Furthermore, the observation that peptides longer than K_4 form aggregates with RNA_{20} suggests that the capacity to form multivalent interactions separates reentrance from aggregation.

References

1. S. Chong *et al.*, Imaging dynamic and selective low-complexity domain interactions that control gene transcription. *Science* **361**, eaar2555 (2018).
2. C. P. Brangwynne *et al.*, Germline P granules are liquid droplets that localize by controlled dissolution/condensation. *Science* **324**, 1729-1732 (2009).
3. Timothy J. Nott *et al.*, Phase Transition of a Disordered Nuage Protein Generates Environmentally Responsive Membraneless Organelles. *Molecular Cell* **57**, 936-947 (2015).
4. S. Maharana *et al.*, RNA buffers the phase separation behavior of prion-like RNA binding proteins. *Science* **360**, 918-921 (2018).
5. A. Molliex *et al.*, Phase separation by low complexity domains promotes stress granule assembly and drives pathological fibrillization. *Cell* **163**, 123-133 (2015).
6. W. Xing, D. Muhlrad, R. Parker, M. K. Rosen, A quantitative inventory of yeast P body proteins reveals principles of composition and specificity. *eLife* **9**, e56525 (2020).
7. S. F. Banani *et al.*, Genetic variation associated with condensate dysregulation in disease. *Dev Cell* **57**, 1776-1788 e1778 (2022).
8. D. T. McSwiggen, M. Mir, X. Darzacq, R. Tjian, Evaluating phase separation in live cells: diagnosis, caveats, and functional consequences. *Genes Dev* **33**, 1619-1634 (2019).
9. T. Mittag, R. V. Pappu, A conceptual framework for understanding phase separation and addressing open questions and challenges. *Mol Cell* **82**, 2201-2214 (2022).
10. P. J. Flory, Thermodynamics of high polymer solutions. *The Journal of chemical physics* **10**, 51-61 (1942).
11. M. L. Huggins, Some properties of solutions of long-chain compounds. *The Journal of Physical Chemistry* **46**, 151-158 (1942).
12. Clifford P. Brangwynne, P. Tompa, Rohit V. Pappu, Polymer physics of intracellular phase transitions. *Nature Physics* **11**, 899-904 (2015).
13. R. K. Das, K. M. Ruff, R. V. Pappu, Relating sequence encoded information to form and function of intrinsically disordered proteins. *Curr Opin Struct Biol* **32**, 102-112 (2015).
14. E. W. Martin *et al.*, Valence and patterning of aromatic residues determine the phase behavior of prion-like domains. *Science* **367**, 694-699 (2020).
15. J. Wang *et al.*, A Molecular Grammar Governing the Driving Forces for Phase Separation of Prion-like RNA Binding Proteins. *Cell* **174**, 688-699 e616 (2018).
16. P. Li *et al.*, Phase transitions in the assembly of multivalent signalling proteins. *Nature* **483**, 336-340 (2012).
17. T. S. Harmon, A. S. Holehouse, M. K. Rosen, R. V. Pappu, Intrinsically disordered linkers determine the interplay between phase separation and gelation in multivalent proteins. *Elife* **6**, (2017).
18. S. F. Banani *et al.*, Compositional Control of Phase-Separated Cellular Bodies. *Cell* **166**, 651-663 (2016).
19. M. T. Wei *et al.*, Phase behaviour of disordered proteins underlying low density and high permeability of liquid organelles. *Nat Chem* **9**, 1118-1125 (2017).
20. S. Alberti, A. Gladfelter, T. Mittag, Considerations and Challenges in Studying Liquid-Liquid Phase Separation and Biomolecular Condensates. *Cell* **176**, 419-434 (2019).
21. J.-M. Choi, A. S. Holehouse, R. V. Pappu, Physical Principles Underlying the Complex Biology of Intracellular Phase Transitions. *Annual Review of Biophysics* **49**, 107-133 (2020).
22. A. Borgia *et al.*, Extreme disorder in an ultrahigh-affinity protein complex. *Nature* **555**, 61-66 (2018).

23. A. Sottini *et al.*, Polyelectrolyte interactions enable rapid association and dissociation in high-affinity disordered protein complexes. *Nat Commun* **11**, 5736 (2020).
24. S. S. Stadmiller, J. S. Aguilar, C. A. Waudby, G. J. Pielak, Rapid Quantification of Protein-Ligand Binding via 19F NMR Lineshape Analysis. *Biophysical Journal* **118**, 2537-2548 (2020).
25. I. Jarmoskaite, I. AlSadhan, P. P. Vaidyanathan, D. Herschlag, How to measure and evaluate binding affinities. *eLife* **9**, e57264 (2020).
26. F. P. Cakmak, S. Choi, M. O. Meyer, P. C. Bevilacqua, C. D. Keating, Prebiotically-relevant low polyion multivalency can improve functionality of membraneless compartments. *Nature Communications* **11**, 5949 (2020).
27. G. Krainer *et al.*, Reentrant liquid condensate phase of proteins is stabilized by hydrophobic and non-ionic interactions. *Nature Communications* **12**, 1085 (2021).
28. Z. Ou, M. Muthukumar, Entropy and enthalpy of polyelectrolyte complexation: Langevin dynamics simulations. *The Journal of Chemical Physics* **124**, (2006).
29. Kathleen A. Burke, Abigail M. Janke, Christy L. Rhine, Nicolas L. Fawzi, Residue-by-Residue View of In Vitro FUS Granules that Bind the C-Terminal Domain of RNA Polymerase II. *Molecular Cell* **60**, 231-241 (2015).
30. S. Elbaum-Garfinkle *et al.*, The disordered P granule protein LAF-1 drives phase separation into droplets with tunable viscosity and dynamics. *Proceedings of the National Academy of Sciences* **112**, 7189-7194 (2015).
31. H. Zhang *et al.*, RNA Controls PolyQ Protein Phase Transitions. *Molecular Cell* **60**, 220-230 (2015).
32. P. P. Gopal, J. J. Nirschl, E. Klinman, E. L. F. Holzbaur, Amyotrophic lateral sclerosis-linked mutations increase the viscosity of liquid-like TDP-43 RNP granules in neurons. *Proceedings of the National Academy of Sciences* **114**, E2466-E2475 (2017).
33. N. O. Taylor, M.-T. Wei, H. A. Stone, C. P. Brangwynne, Quantifying Dynamics in Phase-Separated Condensates Using Fluorescence Recovery after Photobleaching. *Biophysical Journal* **117**, 1285-1300 (2019).
34. A. W. Folkmann, A. Putnam, C. F. Lee, G. Seydoux, Regulation of biomolecular condensates by interfacial protein clusters. *Science* **373**, 1218-1224 (2021).
35. J. Miné-Hattab *et al.*, Single molecule microscopy reveals key physical features of repair foci in living cells. *eLife* **10**, e60577 (2021).
36. N. Galvanetto *et al.*, Extreme dynamics in a biomolecular condensate. *Nature*, (2023).
37. C. Roden, A. S. Gladfelter, RNA contributions to the form and function of biomolecular condensates. *Nature Reviews Molecular Cell Biology* **22**, 183-195 (2021).
38. Y. Shin, C. P. Brangwynne, Liquid phase condensation in cell physiology and disease. *Science* **357**, (2017).
39. K. Besteman, K. Van Eijk, S. G. Lemay, Charge inversion accompanies DNA condensation by multivalent ions. *Nature Physics* **3**, 641-644 (2007).
40. A. N. Milin, A. A. Deniz, Reentrant Phase Transitions and Non-Equilibrium Dynamics in Membraneless Organelles. *Biochemistry* **57**, 2470-2477 (2018).
41. F. Zhang *et al.*, Reentrant Condensation of Proteins in Solution Induced by Multivalent Counterions. *Physical Review Letters* **101**, 148101 (2008).
42. T. T. Nguyen, I. Rouzina, B. I. Shklovskii, Reentrant condensation of DNA induced by multivalent counterions. *The Journal of Chemical Physics* **112**, 2562-2568 (2000).
43. P. R. Banerjee, A. N. Milin, M. M. Moosa, P. L. Onuchic, A. A. Deniz, Reentrant Phase Transition Drives Dynamic Substructure Formation in Ribonucleoprotein Droplets. *Angew Chem Int Ed Engl* **56**, 11354-11359 (2017).
44. S. F. Banani, H. O. Lee, A. A. Hyman, M. K. Rosen, Biomolecular condensates: organizers of cellular biochemistry. *Nat Rev Mol Cell Biol* **18**, 285-298 (2017).

45. A. W. Fritsch *et al.*, Local thermodynamics govern formation and dissolution of *Caenorhabditis* elegans P granule condensates. *Proceedings of the National Academy of Sciences* **118**, e2102772118 (2021).
46. S. Sridharan *et al.*, Systematic discovery of biomolecular condensate-specific protein phosphorylation. *Nature Chemical Biology* **18**, 1104-1114 (2022).
47. A. Bremer *et al.*, Deciphering how naturally occurring sequence features impact the phase behaviours of disordered prion-like domains. *Nat Chem* **14**, 196-207 (2022).
48. J. A. Riback *et al.*, Composition-dependent thermodynamics of intracellular phase separation. *Nature* **581**, 209-214 (2020).
49. J. E. Henninger *et al.*, RNA-Mediated Feedback Control of Transcriptional Condensates. *Cell* **184**, 207-225.e224 (2021).
50. M. Muthukumar, 50th Anniversary Perspective: A Perspective on Polyelectrolyte Solutions. *Macromolecules* **50**, 9528-9560 (2017).
51. J.-M. Choi, F. Dar, R. V. Pappu, LASSI: A lattice model for simulating phase transitions of multivalent proteins. *PLOS Computational Biology* **15**, e1007028 (2019).
52. J. A. Morin *et al.*, Sequence-dependent surface condensation of a pioneer transcription factor on DNA. *Nature Physics* **18**, 271-276 (2022).
53. M. Hofweber, D. Dormann, Friend or foe-Post-translational modifications as regulators of phase separation and RNP granule dynamics. *J Biol Chem* **294**, 7137-7150 (2019).
54. E. Buratti, TDP-43 post-translational modifications in health and disease. *Expert Opin Ther Targets* **22**, 279-293 (2018).
55. C. Despres *et al.*, Identification of the Tau phosphorylation pattern that drives its aggregation. *Proceedings of the National Academy of Sciences* **114**, 9080-9085 (2017).

Acknowledgements: Many thanks to Mariane Le Fur for technical guidance and Alykhan Shamji for thoughts on the manuscript.

Funding: This work was supported by a grant from the National Institutes of Health (R01CA241179) and utilized equipment funded by the Massachusetts Life Science Center.

Competing interests: No conflicts of interest are declared.

Data and materials availability: All data are available in the main text or the supplementary materials. All materials are commercially available.

Supplementary Materials

Methods and Materials

Figs. S1 to S10

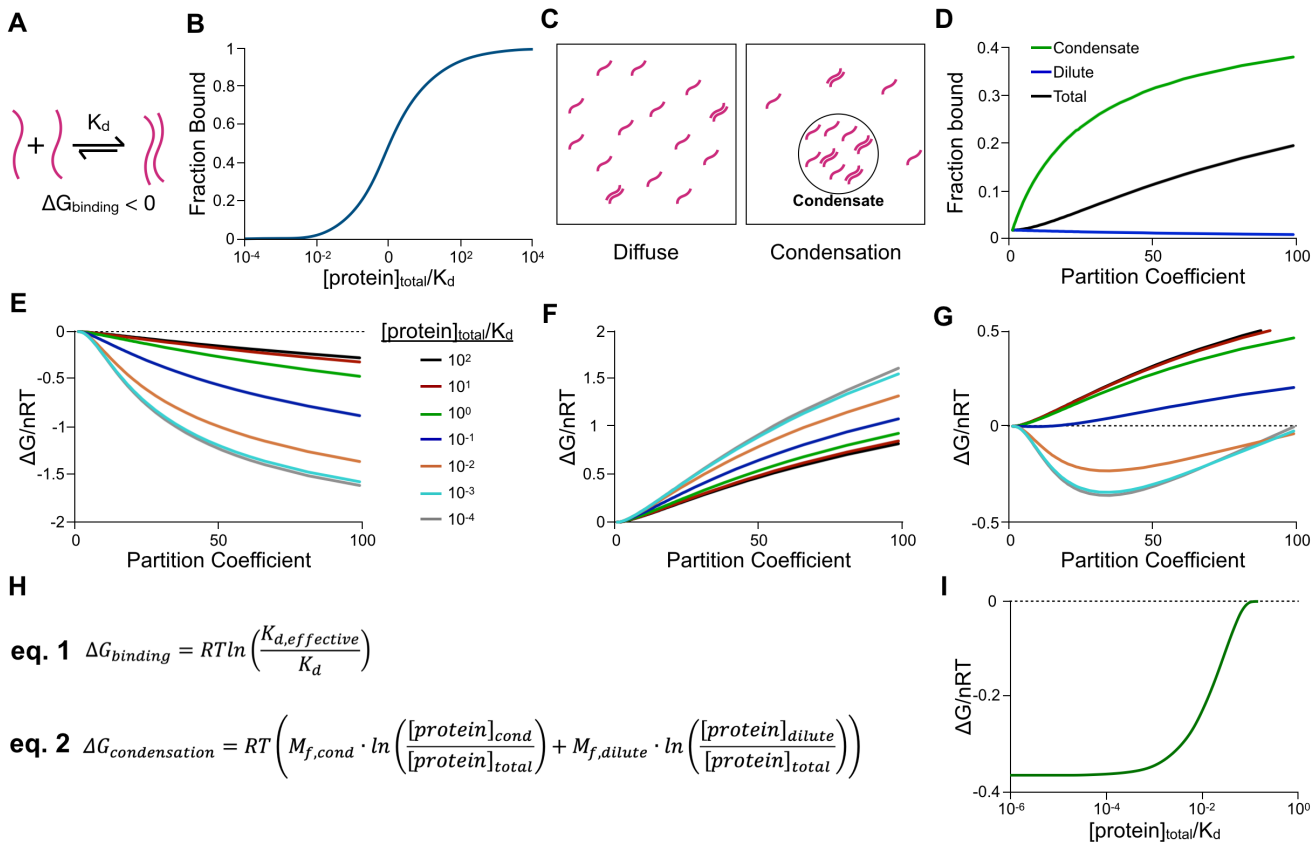

Figure 1. Energetic thermodynamics of the binding model. (**A**) Binding affinity between two molecules is defined by the steady state dissociation constant (K_d) and occurs from a decrease in free energy in the bound state. (**B**) The steady state fraction bound as a function of the $[protein]_{total}/K_d$ ratio. (**C**) Demonstration of a higher bound fraction that occurs within a condensate. (**D**) The fraction bound of a molecule in the condensate (green), dilute region (blue) and the total fraction bound of the system (black) as a function of partition coefficient, shown are calculations at $[protein]_{total}/K_d = 10^{-2}$. (**E**) Change in the free energy of binding upon condensate formation as a function of condensate partition coefficient. (**F**) Change in free energy from the loss of entropy upon condensation as a function of partition coefficient. (**G**) Change in total free energy upon condensate formation as a function of partition coefficient. (**H**) Equations 1 and 2, $M_{f,cond}$ is the mole fraction in the condensate, $M_{f,dilute}$ is the mole fraction in the dilute region. (**I**) The change in free energy minimum upon condensate formation as a function of $[protein]_{total}/K_d$. For all calculations K_d = 1 mM and volume fraction = 1%.

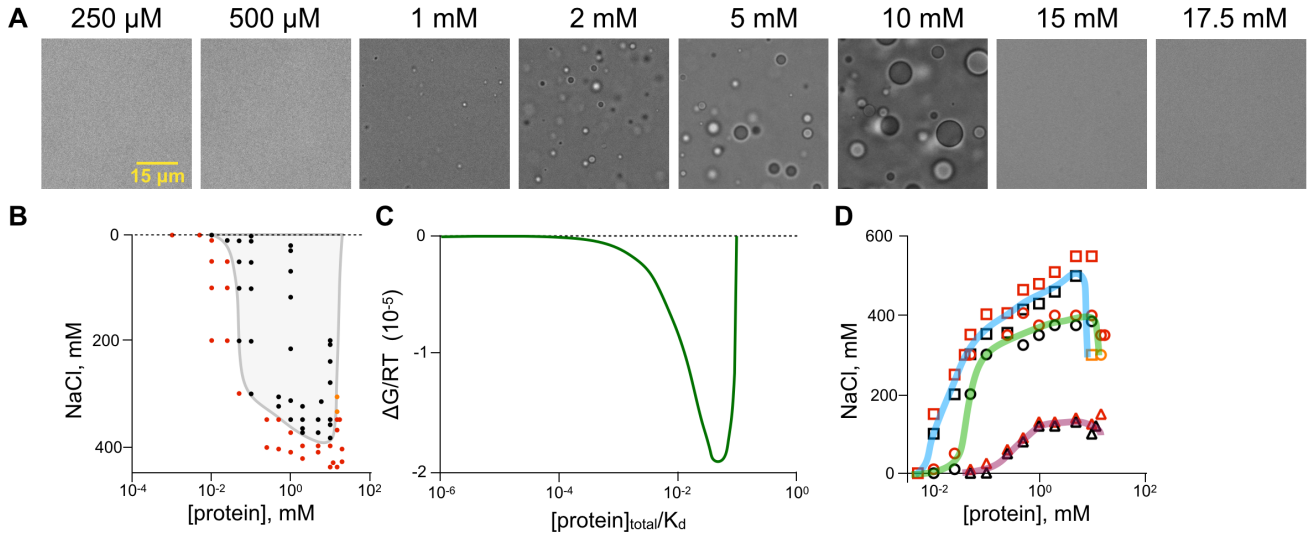

Figure 2. Experimental condensates show reentrance predicted by the binding model. (**A**) Representative DIC images of K_{20}-E_{20} peptide condensates at equimolar concentrations in the presence of 350 mM NaCl. (**B**) Formation (black) or absence (red) of K_{20}-E_{20} condensates at varying NaCl concentrations and equimolar peptide concentrations. A trace between the presence and absence of condensates highlights condensate forming conditions. (**C**) The calculated molar total change in free energy upon condensate formation as a function of $[\text{protein}]_{total}/K_d$, K_d = 1 mM and volume fraction = 1%. (**D**) Presence (black) and absence (red) of condensates for K_{20}-$E2_0$ (circles – green trace), K_{30}-E_{30} (squares – blue trace) and K_{10}-D_{10} (triangles – purple trace) with trace of the boundary for condensate reentrance as a function of [NaCl] and equimolar peptide concentration.

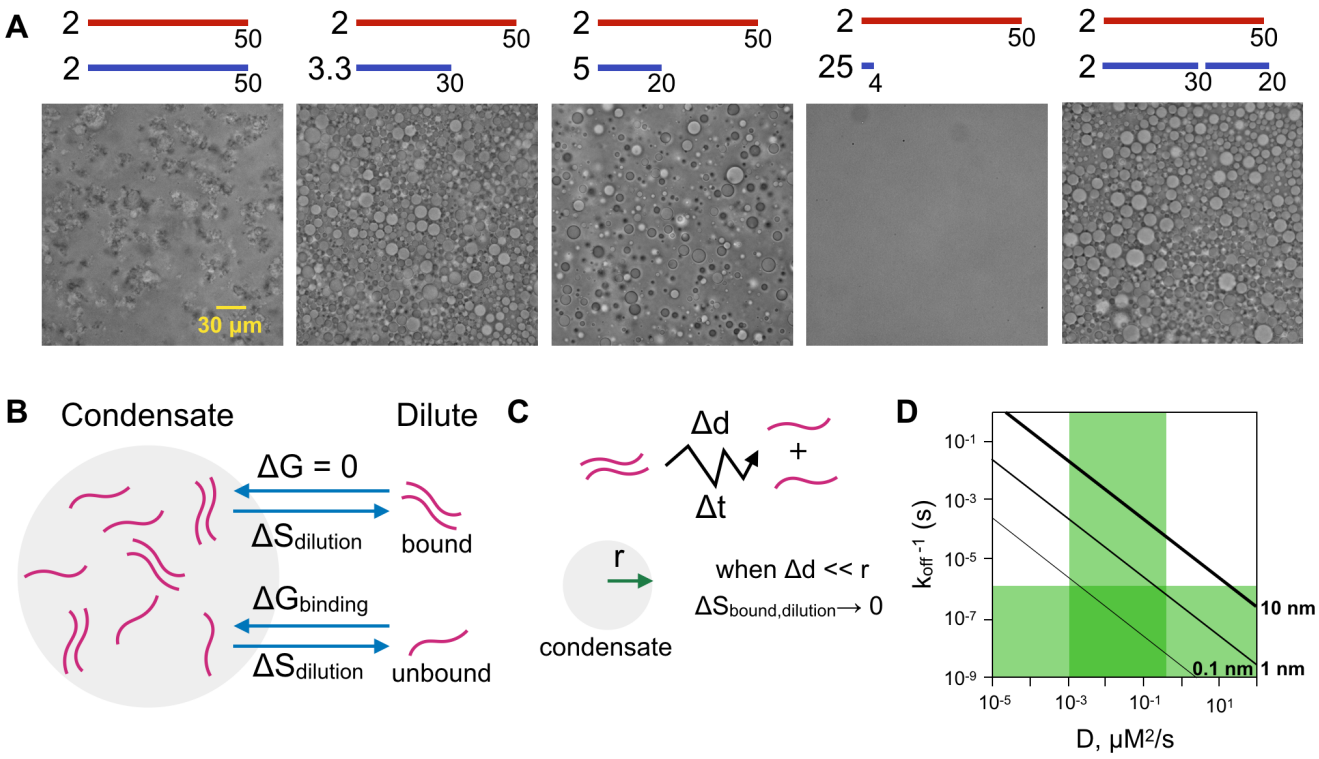

Figure 3. Binding dynamics in condensates. (**A**) Representative DIC images of K_{50} (red) and polyE (blue) at equal charge ratios and 100 mM NaCl, shown are concentrations in mM. (**B**) The energetic

forces impacting on bound and unbound molecules that form condensates. (**C**) The dissociation rate and diffusivity govern the diffusion distance of a bound molecule. (**D**) Reported (green) dissociation rates of intrinsically disordered proteins in condensates and diffusivity measured in condensates. Isolines (black) are plotted for average diffusion distance before dissociation.

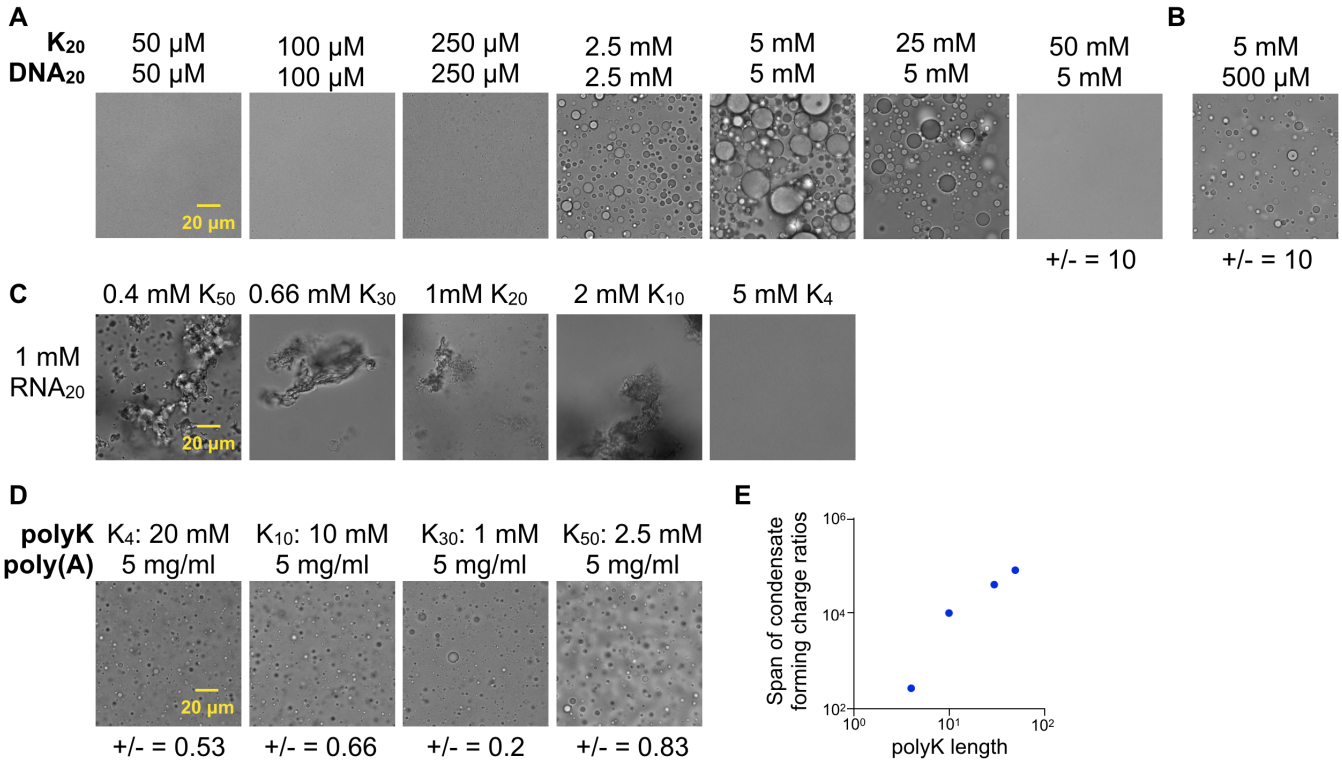

Figure 4. Condensates formed by peptides and oligonucleotides follow the binding model. (**A**) Representative DIC images of K_{20}-DNA_{20} mixtures. (**B**) Representative DIC image of a K_{20}-DNA_{20} mixture at equal charge ratio as the highest concentration in (A). (**C**). Representative DIC images of polyK-RNA_{20} mixtures. (**D**) Representative DIC images of polyK and poly(A) mixtures. (**E**) The charge ratio span (fold difference between high and low) for polyK and poly(A) mixtures over which condensates form as a function of polyK peptide length.